Research Article | Vol. 11, No. 8 / 1 August 2020 / Biomedical Optics Express 4835
Biomedical Optics EXPRESS

In vivo longitudinal visualization of the brain neuroinflammatory response at the cellular level in LysM-GFP mice induced by 3-nitropropionic acid

JINGU LEE,[1,2] EUNJI KONG,[2,3] SUJUNG HONG,[1,2] JIEUN MOON,[1,2] AND PILHAN KIM[1,2,3,*]

[1]*Graduate School of Nanoscience and Technology, Korea Advanced Institute of Science and Technology (KAIST), 291 Daehak-ro, Yuseong-gu, Daejeon 34141, South Korea*
[2]*KI for Health Science and Technology (KIHST), Korea Advanced Institute of Science and Technology (KAIST), 291 Daehak-ro, Yuseong-gu, Daejeon 34141, South Korea*
[3]*Graduate School of Medical Science and Engineering, Korea Advanced Institute of Science and Technology (KAIST), 291 Deahak-ro, Yuseong-gu, Daejeon 34141, South Korea*
[*]*pilhan.kim@kaist.ac.kr*

Abstract: Blood-brain barrier (BBB) dysfunction is related to the development of neuroinflammation in the central nervous system (CNS). Neuroinflammation has been implicated as one of the key factors in the pathogenesis of neurodegenerative diseases such as Alzheimer's disease, Huntington's disease, and Parkinson's disease. Despite its importance, the impacts and underlying cellular mechanisms of chronic BBB impairment in neurodegenerative diseases are poorly understood. In this work, we performed a longitudinal intravital brain imaging of mouse model with neuroinflammation induced by 3-nitropropionic acid (3-NP). For this, we obtained a transgenic LysM-GFP mouse expressing the green fluorescence protein (GFP) in a subset of leukocytes. By using intravenously injected fluorescence blood tracers, we longitudinally observed *in vivo* dynamic cellular behaviors and the BBB integrity through a 30-day neuroinflammatory state. Vascular leakages in the cerebral cortex reflecting BBB impairment were observed at two weeks, which persisted to the third week, followed by a severe inflammatory response with massive leukocytes infiltration at day 30. These descriptions can help in the development of novel approaches to treat neurodegenerative conditions.

1. Introduction

Neuroinflammation could be induced by infection or other pathological onsets; the blood-brain barrier (BBB) breakdown and subsequent infiltration of peripheral immune cells into the brain parenchyma were observed [1]. There is increasing evidence that neuroinflammation is one of the key pathophysiological drivers in the development of neurodegenerative diseases including Alzheimer's disease, Huntington's disease, Parkinson's disease, multiple sclerosis, and amyotrophic lateral sclerosis [2]. In neuroinflammation, it has been suggested that various inflammatory mediators and activated immune cells could directly or indirectly trigger neuronal degeneration through glia cell activation, BBB dysfunction, and demyelination by interrupting nervous homeostasis [3]. For example, T and B cells were activated and localized in the brain parenchyma in multiple sclerosis patients [4]. In an Alzheimer's disease mouse model, LFA-1 integrin produced under the influence of the Aβ42 peptide has a role in neutrophil adhesion to the vascular wall and increased extravasation in areas of amyloid deposits [5]. Microglia, the resident macrophages in the central nervous system, have an important role in maintaining neuronal homeostasis by surveillance and synaptic remodeling in healthy conditions. However, pathological triggers and aggravators for microglia activation could lead to chronic inflammation

#393690 https://doi.org/10.1364/BOE.393690
Journal © 2020 Received 26 Mar 2020; revised 14 Jun 2020; accepted 21 Jul 2020; published 31 Jul 2020

Biomedical Optics EXPRESS

and result in neurodegenerative disease [6]. Additionally, functional integrity of brain vessels has been implicated with various neurodegenerative diseases and cognitive disorders. Recent studies reported that a large proportion of dementia patients might have cerebrovascular lesions, but physiological relation of cerebrovascular dysfunction and neurodegenerative disease at the onset of neuroinflammation is unclear yet [7]. Recently, increasing evidence has suggested that neurovascular dysfunction and disruption of the BBB in neuroinflammatory responses may precede, accelerate, or contribute to neurodegenerative diseases [8,9]. However, the association between vascular alteration and the onset of neuroinflammation has not been well understood in regard to when they are affected and how they respond to pathologic stimulus.

The neuroinflammatory response in neurodegenerative diseases has been investigated using various preclinical animal models [10–12]. There are two types of models: a genetically-modified animal model and a chemically-induced animal model. Commonly used genetically-modified mouse models include APP/PS1 [13] and 5XFAD [14] for Alzheimer's disease, α-synuclein model [15] for Parkinson's disease, and R6/2 mouse model [16] for Huntington's disease, which have been widely used to investigate various pathological features such as impaired cognitive behaviors. Unfortunately, the genetically-modified models require quite a long time to manifest disease-specific symptoms from the birth; it ranges from several months to one year. Thus, it is difficult to investigate the brain at the exact moment when the neuroinflammatory response is triggered and subsequently dissect cellular-level changes with vascular abnormalities over time. In comparison, the chemically-induced animal models have several advantages over the genetically-modified model; the time of onset of neuroinflammation can be controlled, and the disease-specific symptoms manifest at much earlier time-point.

In this work, we used a chemical-induced chronic neuroinflammation mouse model using 3-Nitropropionic acid (3-NP), a neurotoxin, which induces memory/cognition dysfunction with increased oxidative stress [12,17,18]. Using a custom-built intravital laser-scanning confocal microscope system [19–24], we achieved a longitudinal visualization of the cellular-level dynamic responses such as leukocyte infiltration and vascular alteration in the brain parenchyma from the onset of neuroinflammation by 3-NP injection up to 30 days. With the longitudinal imaging, we successfully observed vascular leakages at the capillary level in the cerebral cortex at 2 to 3 weeks, which later triggered a massive leukocyte infiltration into the cortex parenchyma at the same sites at 30 days.

2. Materials and methods

2.1. Animal model

All animal experiments were performed in accordance with the standard guidelines for the care and use of laboratory animals and were approved by the Institutional Animal Care and Use Committee (IACUC) of KAIST (approval No. KA2017-03). Mice were housed and bred in an institutional animal facility in Korea Advanced Institute of Science and Technology (KAIST). All mice were individually housed in ventilated and temperature & humidity-controlled cages (22.5 °C, 52.5%) under 12-12 hours light-dark cycle and provided with standard diet and water ad libitum. For experimental use, 8–12 weeks old male mice (20~30 g) were utilized in this study. Tie2-GFP mice (Stock No. 003658, Jackson Laboratory) where GFP (Green Fluorescence Protein) is expressed under endothelium-specific Tie2 promotor were purchased from the Jackson Laboratory. LysM-GFP mouse [25] expressing GFP in most myelomonocytic cells including neutrophil and macrophage was generously provided by Prof. M. Kim (University of Rochester, USA). A neuroinflammation was induced in mouse model by intraperitoneal injection of 3-NP (20mg/kg; Sigma Aldrich, N5636), which induced a sustained neuroinflammatory response in the brain [12,17,18].

Biomedical Optics EXPRESS

2.2. Intravital imaging system

Custom-built video-rate laser-scanning confocal microscope system previously implemented [19–24] was used as an imaging system to visualize neuroinflammatory response the brain of live mice *in vivo* (Fig. 1(a)). Four continuous-wave laser modules with output wavelengths at 405 nm (OBIS 405, Coherent), 488 nm (MLD488, Cobolt), 561 nm (Jive, Cobolt) and 640 nm (MLD640, Cobolt) were used. A video-rate 2-dimensional laser-scanning at 30 Hz was achieved by using a rotating polygonal mirror (MC-5, aluminum coated, Lincoln Laser) for fast-axis scanning and a galvanometer scanner (6230H, Cambridge Technology) for slow-axis scanning. Multi-color fluorescence signals were simultaneously detected by four photomultiplier tubes (PMT; R9110, Hamamatsu) through bandpass filters (FF01-442/46, FF02-525/50, FF01-600/37, FF01-685/40, Semrock). The output signal of PMTs were digitally acquired by using a frame grabber (Solios, Matrox) and a custom-written image acquisition software based on the Matrox Imaging Library (MIL9, Matrox) for the real-time image display and recording.

2.3. Imaging window preparation

Thinned skull cranial window technique [26] or chronic cranial imaging window method [27] were utilized for intravital imaging of neuroinflammatory process in mice brain *in vivo* (Figs. 1(b)–1(c)). All windows were implemented on the middle of parietal bone covering somatosensory cortex or posterior parietal association area. To implement thinned skull cranial window [26], cranial bone of mouse anesthetized by intraperitoneal injection of Zoletile (20 mg/kg) and Xylazine (10 mg/kg) mixture was surgically exposed by skin incision and subsequent removal of thin translucent connective tissue covering the cranial bone. Small area of the exposed cranial bone (typically 2-3 mm in diameter) was gradually ground by using a high-speed dental drill (Strong 207A, Saeshin) under dissecting microscope. During the grinding process, saline was continuously applied to prevent excessive heating of the bone and potential damage to the underlying brain tissue. The final thickness of the cranial bone after grinding was approximately 20 μm, which allow clear observation of the underlying brain pial vessels (Fig. 1(b)). In addition, a circular-shaped cover glass with diameter of 3 mm (64-0726, Warner Instruments) was attached over the thinned skull by using cyanoacrylate glue. After the surgical procedure, mice were placed in cage to allow full recovery and observed for at least 1 week before being used in imaging experiment. To prepare the chronic cranial imaging window [27], after the surgical exposure of cranial bone by skin incision and connective tissue removal, brain was exposed by making a circular-shaped hole in the cranial bone (typically 3 mm in diameter) with the dental drill under dissecting microscope. Cover glass was attached to the cranial bone to cover the exposed brain by using a fast-curing adhesive (Loctite 401. Henkel). To protect the incision area, dental acrylic resin was used to cover the area except the cover glass. After the surgical procedure, mice were fully recovered for 4 weeks, and mice with clear view of brain through the imaging window like photos in Figs. 1(b)–1(c) were selected and used for intravital imaging.

2.4. Intravital imaging of brain

Mice were anesthetized by intraperitoneal injection of Zoletile (20 mg/kg) and Xylazine (10 mg/kg) mixture and mounted on a stereotaxic plate (US-R-10, Live Cell Instrument) with heating function to maintain the body temperature at 36.5 °C during intravital imaging. To visualize $CD45^+$ leukocytes with fluorescent labeling, 25 μg of anti-CD45 antibody (BD bioscience, 553076) conjugated with Alexa Fluor 647 (Invitrogen, A20006) was intravenously injected at 24 hours before imaging. Similarly, to visualize brain vasculature, endothelial cells were labeled at 24 hours before imaging by intravenously injecting 80 μg of DyLight 649 labelled tomato lectin (Vector Laboratories, DL-1178). Otherwise, blood vessel lumen was visualized by intravenously injecting 35-45 μl of Evans blue (2% wt./vol., Sigma Aldrich, E2129) or 100 μl of Tetramethylrhodamine isothiocyanate-Dextran (TRITC-dextran; 5 mg/ml in saline; Sigma

Biomedical Optics EXPRESS

Aldrich, T1287) right before imaging. Apoptotic cells were labeled at 2 hours before imaging by intravenously injecting 5 μg of Annexin V (BD bioscience, 556416) conjugated with Alexa 555 (Invitrogen, A20009). For longitudinal cellular-level visualization of neuroinflammatory response, repetitive intravital imaging was performed at same locations in the thinned skull or cranial window for 1-4 weeks. Time lapse movies were acquired at randomly selected multiple locations for 10 minutes.

2.5. Imaging analysis

To analyze leukocyte infiltration and brain vessel alteration, z-stack images for 4 weeks were reconstructed into 3-dimensional images by using a commercial image processing software, IMARIS (Bitplane). Average velocity of $LysM^+$ cells in the time-lapse videos were quantified by using track analysis of IMARIS. The number and distribution of infiltrated $LysM^+$ cells and apoptotic cells were measured by 3-dimensional reconstruction and spot analysis of IMARIS. For statistical analysis, all quantification data were statistically analyzed by t-test, and statistical significance was set at $p<0.05$.

3. Results

3.1. Longitudinal repetitive intravital imaging of the neuroinflammation mouse model induced by 3-NP

The neuroinflammation mouse model was induced by intraperitoneal injection of 3-NP (20 mg/kg) into a Tie2-GFP mouse expressing GFP in endothelial cells. In the control mouse, a small number of $CD45^+$ leukocytes were observed in the parenchymal area of the brain meninges. In contrast, in the 3-NP injected mouse, a significantly increased the number of $CD45^+$ leukocytes attached to the blood vessels or infiltrated into the parenchyma of the brain meninges were observed at 7 days after the 3-NP injection, suggesting active recruitment of leukocytes induced by 3-NP (Figs. 1(d)–1(e)).

To further investigate the sustained dynamic cellular-level neuroinflammatory response in the brain, we performed a longitudinal intravital imaging of a 3-NP injected LysM-GFP mouse [25] expressing GFP in neutrophils and in subsets of macrophages and monocytes. By using the thinned skull cranial window method [26], we successfully achieved a repetitive visualization of the same brain area from day 1 to day 10 with a 3-day interval after the 3-NP injection (Fig. 2). In the control mouse, only a small number of $LysM^+$ cells were observed. The number and distribution of the $LysM^+$ cells remained almost similar during the repetitive imaging over 10 days, and there were no observable changes in the brain blood vessels visualized by intravenously injected TRITC-dextran (Fig. 2(a)–2(b)). In the 3-NP injected mouse, at day 1, numerous $LysM^+$ cells were observed infiltrated into the brain presumably actively recruited through the circulation (Fig. 2(a)). Most of the $LysM^+$ cells were located in the perivascular area with a relatively uniform distribution pattern over the imaged brain area. Interestingly, at day 4, a highly dynamic rearrangement was observed in the distribution pattern of the infiltrated $LysM^+$ cells (Figs. 2(a), 2(c), 2(d)). Depending on the observed sites, both the sustained accumulation of infiltrated $LysM^+$ cells until day 10 (Fig. 2(c)) and the disappearance of the initially infiltrated $LysM^+$ cells from day 4 (Fig. 2(d)) were observed. The increased number of infiltrated $LysM^+$ cells in the brain of 3-NP injected mice compared to the control mice was maintained at a similar level from day 1 to day 10, suggesting persistent neuroinflammation (Fig. 2(e)). In contrast, the number of $LysM^+$ cells in the peripheral tissue, ear skin, or abdominal organ, liver of the 3-NP injected mice compared to the control mice were not increased at day 10 (Figs. 2(f)–2(g)).

Biomedical Optics EXPRESS

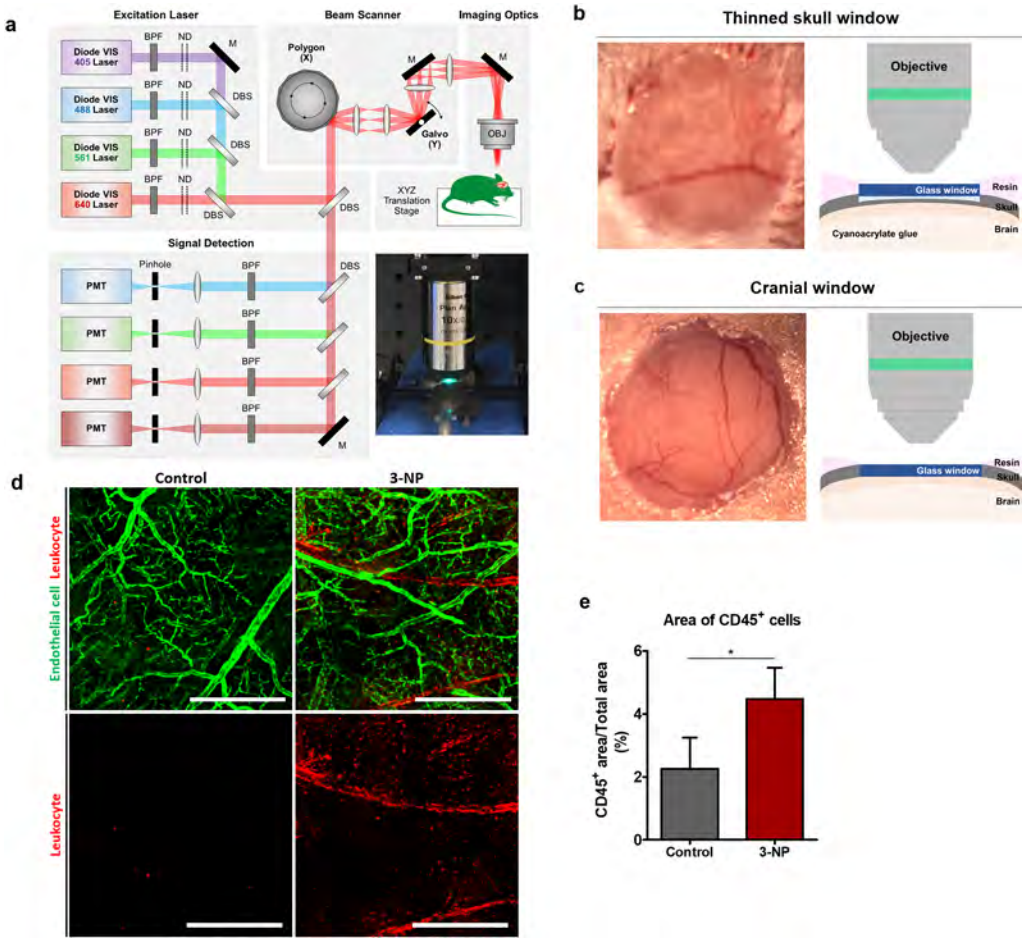

Fig. 1. (a) Schematic of custom-built video-rate laser-scanning confocal microscopy system (ND, neutral density filter; DBS, dichroic beam splitter; BPF, band pass filter; M, mirror; PMT, photomultiplier tube; OBJ, objective lens). (b-c) Photo and schematic of (b) thinned skull window and (c) chronic cranial window for intravital imaging of the brain. (d) Representative mosaic images obtained through the thinned skull of the Tie2-GFP mice *in vivo*; saline-injected control group and 3-NP injected group (green, Tie2-GFP expressed in vascular endothelial cells; red, leukocytes labelled by anti-CD45 antibody conjugated with Alexa 647). (e) Ratio of $CD45^+$ cell occupied area over total imaged area in the control group (n = 4 field of views from 4 mice) and 3-NP group (n = 4 field of views from 4 mice). Scale bars = 500 μm.

Biomedical Optics EXPRESS

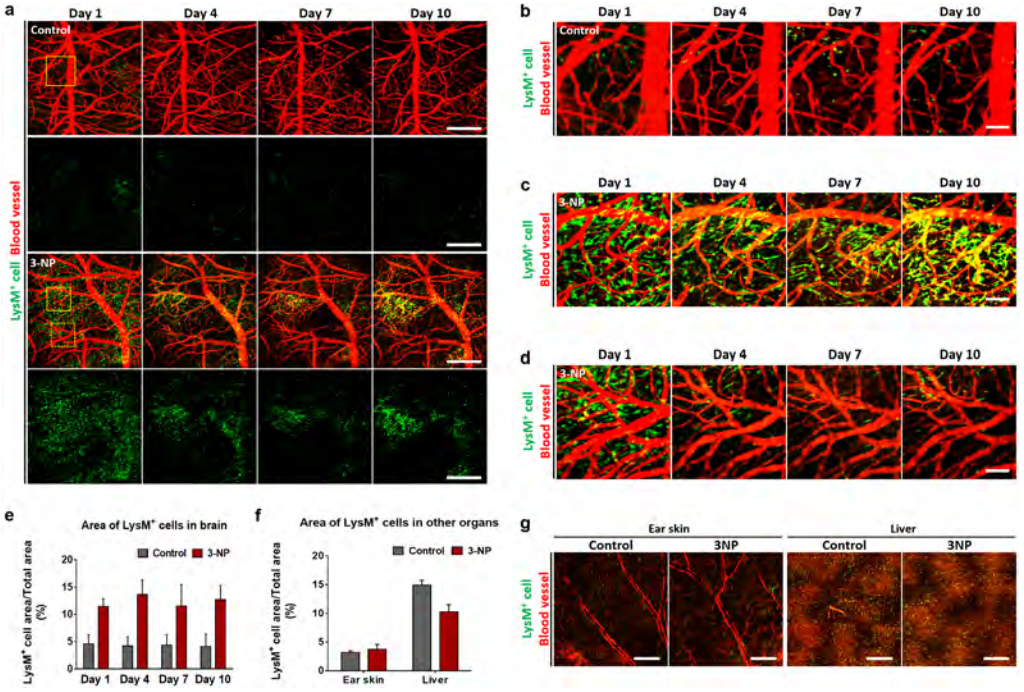

Fig. 2. (a) Representative longitudinal mosaic images obtained through the chronic cranial window implanted in the LysM-GFP mice *in vivo* for 10 days; saline-injected control group (n=3) and 3-NP injected group (n=3) (green, LysM$^+$ cell; red, blood vessel labelled by TRITC-dextran). (b) Magnified longitudinal images of the control group marked by a solid-line square in (a). (c-d) Magnified longitudinal images of the 3-NP group showing a dynamic redistribution of LysM$^+$ cells; (c) sustained accumulation marked by a solid square in (a), (d) disappearance marked by a dotted square in (a). (e-f) Increased area of LysM+ cells in the brain of the control group and 3-NP injected group quantified from the longitudinal mosaic images (n = 3 field of views from 3 mice). (f-g) Comparison of LysM+ cells in non-CNS tissues, ear skin and liver, in the control group and 3-NP injected group; (f) area of LysM+ cells, (g) mosaic images. Scale bars = (a, g) 500 μm, (b-d) 100 μm.

3.2. *Intravital imaging of cellular-level dynamic behaviors of LysM$^+$ cells*

To observe the cellular-level dynamics of LysM$^+$ cells in the brain meningeal vessels and parenchyma in the persistent neuroinflammatory condition, we performed time-lapse imaging in the brain of 3-NP injected LysM-GFP mice through the thinned skull at day 10 after the injection of 3-NP (Visualization 1). The obtained time-lapse movie showed a crawling behavior of the LysM$^+$ cells inside the blood vessel walls whose tracks were marked by dotted lines (Figs. 3(a), 3(b), arrowhead). Additionally, turning and meandering behaviors of the LysM$^+$ cells in the brain parenchyma were observed, and their tracks were marked by solid lines (Fig. 3(a), 3(c), arrow). While we can observe a greatly increased number of LysM$^+$ cells in the brain of the 3-NP injected mice shown in Fig. 2, the average velocity of the crawling LysM$^+$ cells observed in the brain blood vessels and the meandering LysM$^+$ cells in the brain parenchyma showed no difference between the control and 3-NP injected group at day 10 in a persistent neuroinflammation state (Figs. 3(d)–3(e)).

Biomedical Optics EXPRESS

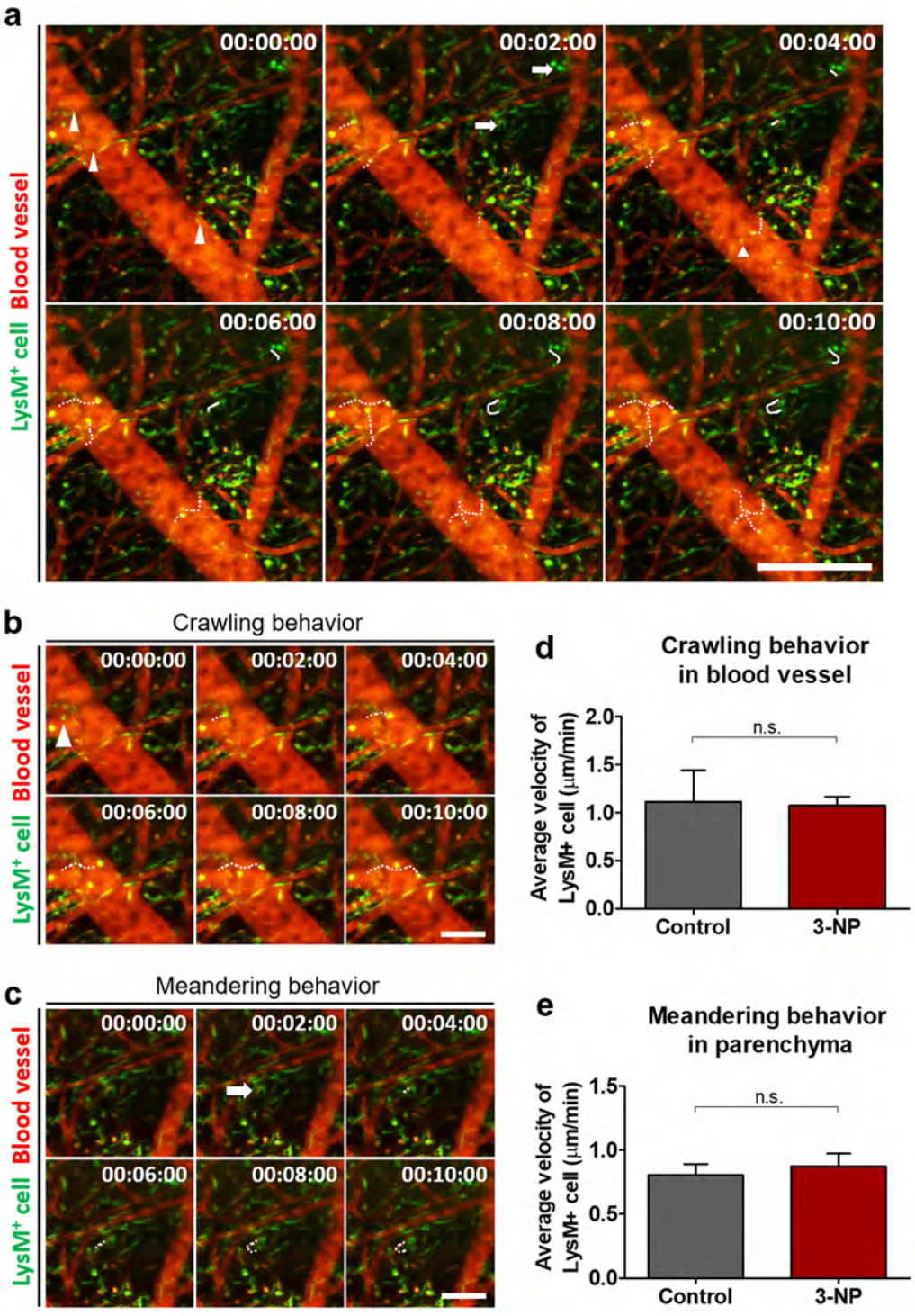

Fig. 3. (a) Time-lapse images obtained from the brain of the LysM-GFP mouse *in vivo* at 10 days after the 3-NP injection (green, LysM-GFP$^+$; red, blood vessel labelled by TRITC-dextran). LysM+ cells showed an intravascular crawling behavior (arrowhead) and a meandering behavior (arrow) in the parenchyma. (b) Serial images showing the crawling behavior of the LysM$^+$ cells along the blood vessel walls. (c) Serial images showing the meandering behavior of the LysM$^+$ cells infiltrated into the parenchyma. (d) Average velocity of the crawling LysM$^+$ cells in the blood vessels (n = 4 field of views from 2 mice). (e) Average velocity of the meandering LysM$^+$ cells in the parenchyma (n = 4 field of views from 2 mice). Scale bars = (a) 250 μm, (b, c) 100 μm.

Biomedical Optics EXPRESS

3.3. Longitudinal visualization of LysM$^+$ cell infiltration and vascular leakage in the cerebral cortex

To observe longitudinal changes in LysM$^+$ cell infiltration and vascular integrity of the blood-brain barrier (BBB) in the cerebral cortex as distinct from the meninges, we performed a longitudinal repetitive z-stack imaging of the brain of 3-NP injected LysM-GFP mice until 30 days through the implanted chronic cranial imaging window [27]. Because the interface between the pia mater, the innermost layer of the meninges, and the brain cerebral cortex was reported to be located at 15-20 μm from the pial surface in a previous study [28], we focused on imaging the same cerebral cortex area more than 20 μm below the pial surface in a single LysM-GFP mouse by repetitive longitudinal imaging until 30 days after the induction of 3-NP (Fig. 4).

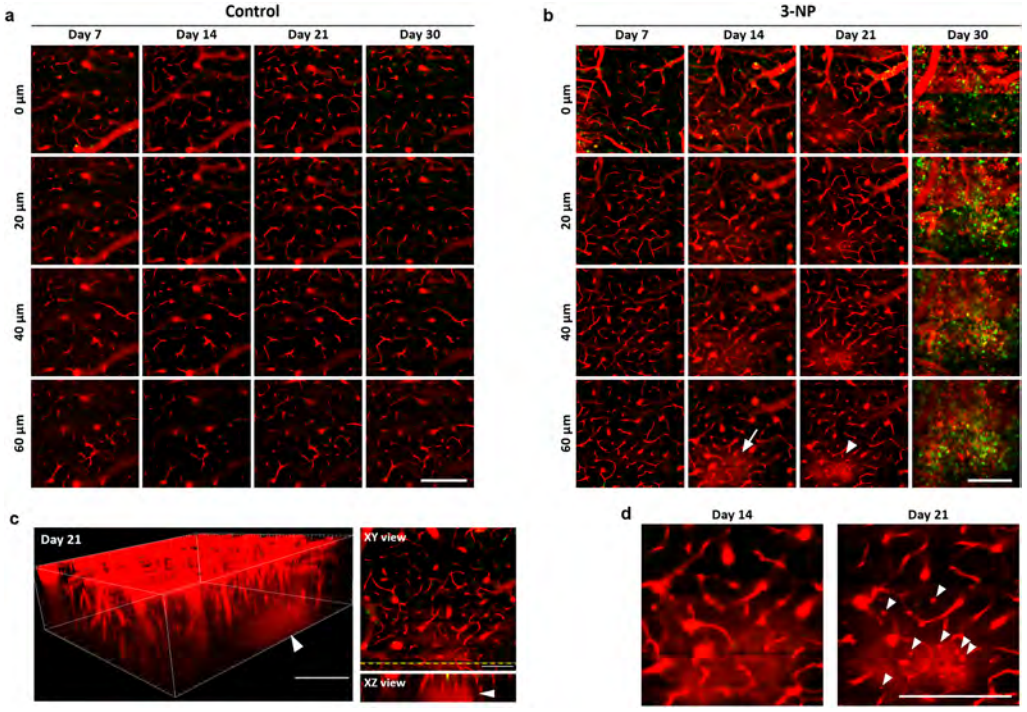

Fig. 4. (a-b) Representative longitudinal z-stack images obtained at the same sites of the brain through a chronic cranial window implanted in LysM-GFP mice *in vivo* for 30 days (green, LysM$^+$ cell; red, blood vessel and vascular leakage labelled by Evans Blue); (a) saline-injected control group (n=2), (b) 3-NP injected group (n=2). (c) 3D rendered image and XY/XZ view image of vascular leakage in the cerebral cortex (arrowhead) reconstructed with the z-stack imaging data obtained at day 21. (d) Repeated observations of the same site in the cerebral cortex with vascular leakage at day 14 and day 21. Small round shaped fluorescent objects (arrowhead) were observed at day 21. Scale bars = (a, b, d) 100 μm, (c) 50 μm.

To visualize vascular leakage indicating a compromised BBB integrity, a far-red fluorophore, Evans blue, was intravenously injected at 30 minutes before every repeated imaging, which has been widely used to visualize blood vessels and monitor the vascular permeability *in vivo* by several optical imaging modalities with its albumin-binding property [29–33]. In the control mouse, no identifiable changes in the vasculature both in morphology and permeability were observed up to 30 days in the entire volume of the cerebral cortex with repetitive imaging through the cranial window (Fig. 4(a)). In the 3-NP injected mouse, at day 7, no vascular leakage was

Biomedical Optics EXPRESS

observed (Fig. 4(b)). However, at day 14, an increased fluorescence signal indicating vascular leakage was observed in the parenchyma of the cerebral cortex at a 60 μm depth (Fig. 4(b), arrow). Interestingly, the vascular leakage was confined to a small volume of the cerebral cortex while blood vessels in other area showed no sign of leakage or morphological changes. At day 21, the vascular leakage was observed at the same area in the cerebral cortex (Figs. 4(b), 4(c), arrowhead), suggesting a persistent compromised BBB integrity. In addition, several small round-shaped fluorescent objects were observed, which were not observed at day 14 when the vascular leakage first observed (Fig. 4(d), arrowhead). They could be infiltrated leukocytes or debris of dead cells labelled by the uptake of leaked Evans blue, suggesting the initiation of the neuroinflammatory response. Finally, at day 30, numerous $LysM^+$ cells were observed that had infiltrated to the same area. Additionally, a large number of accumulated objects labelled by the leaked Evan Blue were observed, which were mostly leukocytes recruited to the area through the breached BBB between day 21 and day 30.

To assess the chronic cytotoxic effect accompanied with the altered vascular integrity by the 3-NP injection, cellular apoptosis and blood vessels in the brain were visualized at day 30 by intravenously injected Annexin V and lectin, respectively (Fig. 5(a)). In the 3-NP injected group, the number of Annexin V^+ apoptotic bodies were greatly increased in comparison with the control group in which far fewer numbers of Annexin V^+ bodies were observed, mostly at the superficial area (Figs. 5(a)–5(b)). Interestingly, in the cerebral cortex below the 20 μm depth, apoptotic bodies were rarely observed in the control group while many apoptotic bodies were observed in the 3-NP injected group occupying 29% of all observed apoptotic bodies. (Figure 5(c)).

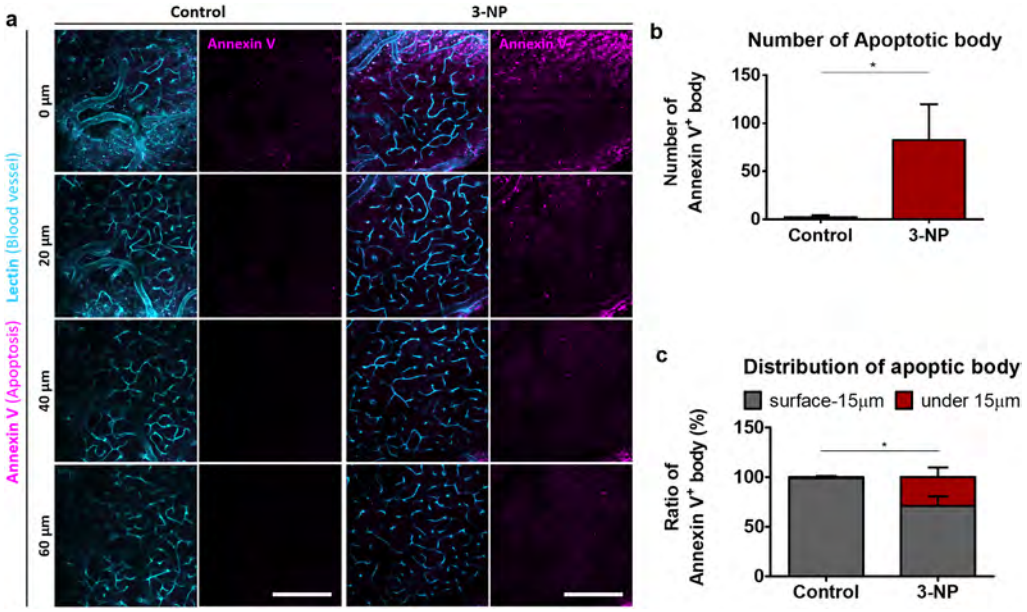

Fig. 5. (a) Z-stack images of the brain obtained at 30 days after saline (control) or 3-NP injection (cyan, lectin conjugated with DyLight 649 labeling blood vessel; Magenta, Annexin V conjugated with Alexa Fluor 555 labeling apoptotic body). (b) Number of Annexin V^+ apoptotic bodies observed in the control group and 3-NP injected group. (c) Ratio of Annexin V^+ apoptotic bodies observed in the superficial area (surface–15 μm) and cerebral cortex (under 15 μm) of the control group and 3-NP injected group. Scale bars = 100 μm

Biomedical Optics EXPRESS

4. Discussion

3-NP, isolated from plants, can irreversibly inhibit the function of succinate dehydrogenase, which participates in the Krebs cycle occurring in mitochondria, affecting the energy metabolism of neurons and consequently leading to neuronal death. In addition, activation of caspases with the overproduction of reactive oxygen species (ROS) and nitric oxide (NO) has been attributed to neuronal death by 3-NP [34]. Previous studies have reported that 3-NP, known as a mitochondrial toxin, could effectively cause behavioral changes and brain damage in animal models, mimicking clinical manifestations of Huntington's disease [17,34]. In addition, some reports have investigated that systemic injection of 3-NP showed silver-impregnated neurons in cortex, striatum, hippocampus and amygdala [35,36], but these neuronal damages and degeneration by 3-NP have been mostly analyzed by histological analysis focusing on the striatum in the subcortical basal ganglia of the brain associated with Huntington's disease. Pathologic changes in the cerebral cortex by 3-NP have been remained mostly unexplored and intravital imaging study has not been performed. We utilized custom-built intravital confocal microscopy system with cranial window technique to longitudinally and repetitively visualize same cerebral cortex volume from the very onset of neuroinflammation by 3-NP up to 30 days and identify the association between BBB leakage and leukocyte infiltration.

In this study, with a chronic cranial window, we successfully performed a repetitive intravital microscopic imaging of the same area in the cerebral cortex and BBB integrity monitoring with Evans blue. Notably, the longitudinal observation clearly revealed that, in the cerebral cortex, 3-NP could induce the disruption of the BBB function shown by the vascular leakage of Evans blue at 2 weeks after injection, which subsequently led to the infiltration of leukocytes including $LysM^+$ cells to the same site. These data show that leukocyte infiltration into cerebral cortex might be essentially associated with the functional deterioration of the BBB in brain vessels. In the more superficial area, the meninges, we observed an immediate neuroinflammatory response manifested by a greatly increased number of infiltrated $LysM^+$ cell after 3-NP injection in 1 day, which persisted until 10 days with the dynamic cellular behaviors of the infiltrated $LysM^+$ cells. It has been reported that the meninges contains numerous immune cells including macrophages, dendritic cells, and lymphocytes, having a role as the first immune defense against injections and neurotoxins [37]. Thus, it could be the result of the reaction of the meninges as a barrier in response to the onset of neuroinflammation induced by 3-NP in the central nervous system (CNS).

Previous *in vivo* imaging studies using brain disease model have shown that various pathological response could be detected by positron emission tomography but not in cellular resolution [38,39]. In the last decade, intravital confocal microscopy system and multi-photon laser scanning microscopy system in combination with surgical techniques have been developed to visualize cellular-level responses in brain disease model with improved field of view as well as imaging quality [40]. To note, previous studies have reported that vascular leakage was related with leukocyte infiltration in skin [41] and tumor [42], and endothelial junction molecules have a role in leukocyte extravasation and vascular permeability [43]. However, a longitudinal high-resolution observation of degradation of BBB function such as vascular leakage and leukocyte infiltration has not been achieved. Our results showed that the sustained neuroinflammation by 3-NP in cerebral cortex could induce vascular leakage and it might trigger leukocyte infiltration into brain parenchyma in time course of 1-2 weeks.

To summarize, our longitudinal imaging of the 3-NP induced neuroinflammation model revealed that the meninges and the cerebral cortex in brain showed temporally different inflammatory responses. Nevertheless, further investigation is needed to answer whether the acute inflammatory response observed in the meninges by 3-NP is related to the later inflammatory response observed in the cerebral cortex or are they independent processes from each other induced by 3-NP. In addition, brain vessels are characterized by a neurovascular unit (NVU) comprising brain

Biomedical Optics EXPRESS

endothelial cells, pericytes, glia, and neurons, which controls the permeability of the BBB tightly regulating the transport of circulating molecules into the brain parenchyma [8,44]. It would be important to observe the cellular- and molecular-level changes in the NVU that occur with the disruption of the BBB induced by 3-NP to further improve our mechanistic understanding about vascular alteration related with neuroinflammation [8,45].

5. Conclusion

In this work, we established a chronic neuroinflammation mouse model induced by 3-NP. Using a custom-built intravital laser-scanning confocal microscope system with chronic brain imaging window techniques, we achieved a longitudinal cellular-level *in vivo* visualization of neuroinflammatory responses in the brain of transgenic LysM-GFP mice from the onset of neuroinflammation by 3-NP injection up to 1 month. In the meninges, numerous $LysM^+$ cells actively infiltrated into the meningeal parenchyma in 1 day. Repeated imaging of the same brain area revealed an active rearrangement of the infiltrated $LysM^+$ cells from day 4 to day 10 with dynamic behaviors such as intravascular crawling and meandering in the parenchyma. Interestingly, in the cerebral cortex, vascular leakage with BBB disruption was observed from 2 weeks after the 3-NP injection. Longitudinal imaging of the same area revealed that the functional impairment of the BBB persisted to 3 weeks and finally resulted in severe inflammation with massive infiltration of $LysM^+$ cells and leukocytes at 1 month. It showed the *in vivo* progression of the BBB dysfunction to neuroinflammation during the time frame of day 14 to day 30 after 3-NP injection. To summarize, these results demonstrate that longitudinal intravital imaging of the 3-NP neuroinflammation model can be a useful approach to further investigate unknown underlying cellular mechanisms related BBB dysfunction and neuroinflammation potentially in neurodegenerative diseases *in vivo*.

Funding

National Research Foundation of Korea (2016M3C7A1913844, 2017R1E1A1A01074190, 2018H1A2A1060332).

Acknowledgements

We would like to thank Dr. M. Kim (University of Rochester, USA) for providing the LysM-GFP mouse.

Disclosures

The authors declare no conflict of interest.

References

1. M. T. Heneka, M. P. Kummer, and E. Latz, "Innate immune activation in neurodegenerative disease," Nat. Rev. Immunol. **14**(7), 463–477 (2014).
2. C. K. Glass, K. Saijo, B. Winner, M. C. Marchetto, and F. H. Gage, "Mechanisms underlying inflammation in neurodegeneration," Cell **140**(6), 918–934 (2010).
3. R. Sankowski, S. Mader, and S. I. Valdes-Ferrer, "Systemic inflammation and the brain: novel roles of genetic, molecular, and environmental cues as drivers of neurodegeneration," Front. Cell. Neurosci. **9**, 28 (2015).
4. R. Schneider, A. N. Mohebiany, I. Ifergan, D. Beauseigle, P. Duquette, A. Prat, and N. Arbour, "B cell-derived IL-15 enhances CD8 T cell cytotoxicity and is increased in multiple sclerosis patients," J. Immunol. **187**(8), 4119–4128 (2011).
5. E. Zenaro, E. Pietronigro, V. Della Bianca, G. Piacentino, L. Marongiu, S. Budui, E. Turano, B. Rossi, S. Angiari, S. Dusi, A. Montresor, T. Carlucci, S. Nani, G. Tosadori, L. Calciano, D. Catalucci, G. Berton, B. Bonetti, and G. Constantin, "Neutrophils promote Alzheimer's disease-like pathology and cognitive decline via LFA-1 integrin," Nat. Med. **21**(8), 880–886 (2015).

Biomedical Optics EXPRESS

6. M. T. Heneka, M. J. Carson, J. El Khoury, G. E. Landreth, F. Brosseron, D. L. Feinstein, A. H. Jacobs, T. Wyss-Coray, J. Vitorica, R. M. Ransohoff, K. Herrup, S. A. Frautschy, B. Finsen, G. C. Brown, A. Verkhratsky, K. Yamanaka, J. Koistinaho, E. Latz, A. Halle, G. C. Petzold, T. Town, D. Morgan, M. L. Shinohara, V. H. Perry, C. Holmes, N. G. Bazan, D. J. Brooks, S. Hunot, B. Joseph, N. Deigendesch, O. Garaschuk, E. Boddeke, C. A. Dinarello, J. C. Breitner, G. M. Cole, D. T. Golenbock, and M. P. Kummer, "Neuroinflammation in Alzheimer's disease," Lancet Neurol. **14**(4), 388–405 (2015).
7. N. The Lancet, "Vascular disease and neurodegeneration: advancing together," Lancet Neurol. **16**(5), 333 (2017).
8. A. R. Nelson, M. D. Sweeney, A. P. Sagare, and B. V. Zlokovic, "Neurovascular dysfunction and neurodegeneration in dementia and Alzheimer's disease," Biochim. Biophys. Acta, Mol. Basis Dis. **1862**(5), 887–900 (2016).
9. B. V. Zlokovic, "The blood-brain barrier in health and chronic neurodegenerative disorders," Neuron **57**(2), 178–201 (2008).
10. D. Krstic, A. Madhusudan, J. Doehner, P. Vogel, T. Notter, C. Imhof, A. Manalastas, M. Hilfiker, S. Pfister, C. Schwerdel, C. Riether, U. Meyer, and I. Knuesel, "Systemic immune challenges trigger and drive Alzheimer-like neuropathology in mice," J. Neuroinflammation **9**(1), 699 (2012).
11. J. W. Lee, Y. K. Lee, D. Y. Yuk, D. Y. Choi, S. B. Ban, K. W. Oh, and J. T. Hong, "Neuro-inflammation induced by lipopolysaccharide causes cognitive impairment through enhancement of beta-amyloid generation," J. Neuroinflammation **5**(1), 37 (2008).
12. P. Kumar and A. Kumar, "Effect of lycopene and epigallocatechin-3-gallate against 3-nitropropionic acid induced cognitive dysfunction and glutathione depletion in rat: a novel nitric oxide mechanism," Food Chem. Toxicol. **47**(10), 2522–2530 (2009).
13. S. J. Webster, A. D. Bachstetter, and L. J. Van Eldik, "Comprehensive behavioral characterization of an APP/PS-1 double knock-in mouse model of Alzheimer's disease," Alzheimer's Res. Ther. **5**(3), 28 (2013).
14. H. Oakley, S. L. Cole, S. Logan, E. Maus, P. Shao, J. Craft, A. Guillozet-Bongaarts, M. Ohno, J. Disterhoft, L. Van Eldik, R. Berry, and R. Vassar, "Intraneuronal beta-amyloid aggregates, neurodegeneration, and neuron loss in transgenic mice with five familial Alzheimer's disease mutations: potential factors in amyloid plaque formation," J. Neurosci. **26**(40), 10129–10140 (2006).
15. S. M. Fleming, J. Salcedo, P. O. Fernagut, E. Rockenstein, E. Masliah, M. S. Levine, and M. F. Chesselet, "Early and progressive sensorimotor anomalies in mice overexpressing wild-type human alpha-synuclein," J. Neurosci. **24**(42), 9434–9440 (2004).
16. S. Ramaswamy, J. L. McBride, and J. H. Kordower, "Animal models of Huntington's disease," ILAR J. **48**(4), 356–373 (2007).
17. M. F. Beal, E. Brouillet, B. G. Jenkins, R. J. Ferrante, N. W. Kowall, J. M. Miller, E. Storey, R. Srivastava, B. R. Rosen, and B. T. Hyman, "Neurochemical and histologic characterization of striatal excitotoxic lesions produced by the mitochondrial toxin 3-nitropropionic acid," J. Neurosci. **13**(10), 4181–4192 (1993).
18. P. O. Fernagut, E. Diguet, N. Stefanova, M. Biran, G. K. Wenning, P. Canioni, B. Bioulac, and F. Tison, "Subacute systemic 3-nitropropionic acid intoxication induces a distinct motor disorder in adult C57Bl/6 mice: behavioural and histopathological characterisation," Neuroscience **114**(4), 1005–1017 (2002).
19. S. Ahn, K. Choe, S. Lee, K. Kim, E. Song, H. Seo, I. Kim, and P. Kim, "Intravital longitudinal wide-area imaging of dynamic bone marrow engraftment and multilineage differentiation through nuclear-cytoplasmic labeling," PLoS One **12**(11), e0187660 (2017).
20. J. Ahn, E. Kong, K. Choe, E. Song, Y. Hwang, H. Seo, I. Park, and P. Kim, "In vivo longitudinal depth-wise visualization of tumorigenesis by needle-shaped side-view confocal endomicroscopy," Biomed. Opt. Express **10**(6), 2719–2729 (2019).
21. I. Park, K. Choe, H. Seo, Y. Hwang, E. Song, J. Ahn, Y. Hwan Jo, and P. Kim, "Intravital imaging of a pulmonary endothelial surface layer in a murine sepsis model," Biomed. Opt. Express **9**(5), 2383–2393 (2018).
22. I. Park, M. Kim, K. Choe, E. Song, H. Seo, Y. Hwang, J. Ahn, S. H. Lee, J. H. Lee, Y. H. Jo, K. Kim, G. Y. Koh, and P. Kim, "Neutrophils disturb pulmonary microcirculation in sepsis-induced acute lung injury," Eur. Respir. J. **53**(3), 1800786 (2019).
23. K. Choe, Y. Hwang, H. Seo, and P. Kim, "In vivo high spatiotemporal resolution visualization of circulating T lymphocytes in high endothelial venules of lymph nodes," J. Biomed. Opt. **18**(03), 1 (2013).
24. H. Seo, Y. Hwang, K. Choe, and P. Kim, "In vivo quantitation of injected circulating tumor cells from great saphenous vein based on video-rate confocal microscopy," Biomed. Opt. Express **6**(6), 2158–2167 (2015).
25. N. Faust, F. Varas, L. M. Kelly, S. Heck, and T. Graf, "Insertion of enhanced green fluorescent protein into the lysozyme gene creates mice with green fluorescent granulocytes and macrophages," Blood **96**(2), 719–726 (2000).
26. G. Yang, F. Pan, C. N. Parkhurst, J. Grutzendler, and W. B. Gan, "Thinned-skull cranial window technique for long-term imaging of the cortex in live mice," Nat. Protoc. **5**(2), 201–208 (2010).
27. A. Holtmaat, T. Bonhoeffer, D. K. Chow, J. Chuckowree, V. De Paola, S. B. Hofer, M. Hubener, T. Keck, G. Knott, W. C. Lee, R. Mostany, T. D. Mrsic-Flogel, E. Nedivi, C. Portera-Cailliau, K. Svoboda, J. T. Trachtenberg, and L. Wilbrecht, "Long-term, high-resolution imaging in the mouse neocortex through a chronic cranial window," Nat. Protoc. **4**(8), 1128–1144 (2009).
28. C. Laperchia, A. L. Allegra Mascaro, L. Sacconi, A. Andrioli, A. Matte, L. De Franceschi, G. Grassi-Zucconi, M. Bentivoglio, M. Buffelli, and F. S. Pavone, "Two-photon microscopy imaging of thy1GFP-M transgenic mice: a novel animal model to investigate brain dendritic cell subsets in vivo," PLoS One **8**(2), e56144 (2013).

Biomedical Optics EXPRESS

29. J. Yao, K. Maslov, S. Hu, and L. V. Wang, "Evans blue dye-enhanced capillary-resolution photoacoustic microscopy in vivo," J. Biomed. Opt. **14**(5), 054049 (2009).
30. K. Choe, J. Y. Jang, I. Park, Y. Kim, S. Ahn, D. Y. Park, Y. K. Hong, K. Alitalo, G. Y. Koh, and P. Kim, "Intravital imaging of intestinal lacteals unveils lipid drainage through contractility," J. Clin. Invest. **125**(11), 4042–4052 (2015).
31. S. Ogura, K. Kurata, Y. Hattori, H. Takase, T. Ishiguro-Oonuma, Y. Hwang, S. Ahn, I. Park, W. Ikeda, S. Kusuhara, Y. Fukushima, H. Nara, H. Sakai, T. Fujiwara, J. Matsushita, M. Ema, M. Hirashima, T. Minami, M. Shibuya, N. Takakura, P. Kim, T. Miyata, Y. Ogura, and A. Uemura, "Sustained inflammation after pericyte depletion induces irreversible blood-retina barrier breakdown," JCI Insight **2**(3), e90905 (2017).
32. W. Liu and J. Yao, "Photoacoustic microscopy: principles and biomedical applications," Open Biomed. Eng. Lett. **8**(2), 203–213 (2018).
33. Y. Li and Z. Chen, "Multimodal Intravascular Photoacoustic and Ultrasound Imaging," Open Biomed. Eng. Lett. **8**(2), 193–201 (2018).
34. W. T. Lee and C. Chang, "Magnetic resonance imaging and spectroscopy in assessing 3-nitropropionic acid-induced brain lesions: an animal model of Huntington's disease," Prog. Neurobiol. **72**(2), 87–110 (2004).
35. P. J. Miller and L. Zaborszky, "3-Nitropropionic acid neurotoxicity: visualization by silver staining and implications for use as an animal model of Huntington's disease," Exp. Neurol. **146**(1), 212–229 (1997).
36. H. Akashiba, Y. Ikegaya, N. Nishiyama, and N. Matsuki, "Differential involvement of cell cycle reactivation between striatal and cortical neurons in cell death induced by 3-nitropropionic acid," J. Biol. Chem. **283**(10), 6594–6606 (2008).
37. A. E. Russi and M. A. Brown, "The meninges: new therapeutic targets for multiple sclerosis," Transl. Res. **165**(2), 255–269 (2015).
38. A. Chaney, S. R. Williams, and H. Boutin, "In vivo molecular imaging of neuroinflammation in Alzheimer's disease," J. Neurochem. **149**(4), 438–451 (2019).
39. J. Lagarde, M. Sarazin, and M. Bottlaender, "In vivo PET imaging of neuroinflammation in Alzheimer's disease," J. Neural Transm. **125**(5), 847–867 (2018).
40. E. Pietronigro, E. Zenaro, and G. Constantin, "Imaging of Leukocyte Trafficking in Alzheimer's Disease," Front. Immunol. **7**, 33 (2016).
41. S. Ono, G. Egawa, and K. Kabashima, "Regulation of blood vascular permeability in the skin," Inflammation Regener. **37**(1), 11 (2017).
42. L. Claesson-Welsh, "Vascular permeability–the essentials," Upsala J. Med. Sci. **120**(3), 135–143 (2015).
43. W. A. Muller, "Leukocyte-endothelial-cell interactions in leukocyte transmigration and the inflammatory response," Trends Immunol. **24**(6), 326–333 (2003).
44. B. V. Zlokovic, "Neurovascular pathways to neurodegeneration in Alzheimer's disease and other disorders," Nat. Rev. Neurosci. **12**(12), 723–738 (2011).
45. A. Varatharaj and I. Galea, "The blood-brain barrier in systemic inflammation," Brain, Behav., Immun. **60**, 1–12 (2017).